Case Studies in Construction Materials 19 (2023) e02567

Contents lists available at ScienceDirect

Case Studies in Construction Materials

journal homepage: www.elsevier.com/locate/cscm

Development of rubberised cementitious material incorporating graphene nanoplatelets and silica fume

Hassan Amer Algaifi [a], Agusril Syamsir [a], Shahrizan Baharom [b,*], Mana Alyami [c,*], Abdo Mohammed Al-Fakih [d], Vivi Anggraini [e]

[a] Institute of Energy Infrastructure (IEI), Universiti Tenaga Nasional, Jalan IKRAM-UNITEN, Kajang 43000, Malaysia
[b] Department of Civil Engineering, Universiti Kebangsaan Malaysia (UKM), Bangi 43600, Selangor, Malaysia
[c] Department of Civil Engineering, College of Engineering, Najran University, Najran, Saudi Arabia
[d] Department of Chemistry, Faculty of Science, Universiti Teknologi Malaysia, Skudai 81310, Johor, Malaysia
[e] Civil Engineering Department, School of Engineering, Monash University Malaysia, Jalan Lagoon Selatan, Bandar Sunway 47500, Selangor Darul Ehsan, Malaysia

ARTICLE INFO

Keywords:
Green cementitious material
Rubberised cementitious material
Graphene-based cementitious material
Propagation of concrete cracks
mechanical properties

ABSTRACT

Rubberised cementitious material has gained significant attention within the civil engineering community. However, the gap and voids between rubber particles and cement gel remain challenge. To tackle these issues, silica fume (SF) and graphene nanoplatelets (GnPs) were used to enhance the microstructure of rubberised mortar at micro and nano scale levels. Silica fume was added at 20% of the cement weight, while, the inoculation of GnPs varied from 0.02% to 0.6% as cement replacement and the rubber powder ranged between 2% and 8% as sand replacement (by volume). The compressive (CS), flexural (FS), tensile (TS), ultrasonic pulse velocity (UPV), water absorption (WA) and porosity (*P*) of the proposed mortar were evaluated at the age of 28 days. The experimental and predicted outcome showed that the rubberised mortar incorporating SF and GnPs imparted superior properties compared to that of the control mixture for all rubber replacement percentage. For instance, when the rubber content was 5% and GnPs was 0.03%, the CS, FS, TS, UPV, WA and *P* were 45.51 MPA, 5.41 MPa, 3.13 MPa, 3.89 km/s, 5.23% and 7.22% compared to that of the control mortar without rubber (38.3 MPa, 4.1 MPa, 2.31 MPa, 3.65 km/s, 6.51% and 7.28%), respectively. FESEM also confirmed that the GnPs did not only acted as a filler material but also served as an impermeable barrier for continued crack propagation. It can be concluded that the inclusion of GnPs in rubberised cement-based material is considered as a sustainable choice in which it enhances its microstructure, specifically the interfacial transition zone (ITZ).

1. Introduction

As a result of rapid urbanisation globally, several serious environmental issues have arisen. The initial serious environmental issue is the increase of uncontrolled waste materials disposal and limited landfill. This concern has since prompted environmentalists and civil engineers to incorporate waste materials in concrete [1–3]. Another serious environmental issue is the rapid construction of new cement-based structures that is dependent on a huge amount of cement, which has also caused grave air pollution owing to the

* Corresponding authors.
E-mail addresses: shahrizan@ukm.edu.my (S. Baharom), mmsalmansour@nu.edu.sa (M. Alyami).

https://doi.org/10.1016/j.cscm.2023.e02567
Received 16 July 2023; Received in revised form 2 October 2023; Accepted 9 October 2023
Available online 11 October 2023

associated emission of carbon dioxide (CO_2) from cement factories. According to the International Energy Agency (IEA), approximately 7% of the total CO_2 emission was linked to cement production [4]. In an effort to tackle these two pressing problems, many researchers have adopted the concept of combining both green and sustainable concrete [5–7]. Green concrete is defined as concrete incorporating waste materials as the replacement of either cement, sand or coarse aggregate, while sustainable concrete is linked to a longer lifespan of concrete that is associated with lower repair cost and lesser maintenance [8].

Focusing on green concrete, rubberised concrete is one of the environmentally friendly materials that were investigated in this present literature. Compared to conventional concrete, it contains crumb rubber, as the partial replacement of either fine or coarse aggregate. Indeed, the reputation of rubberised concrete is rapidly increasing in the civil engineering community in recent years [9, 10]. This is attributed to the fact that reusing discarded rubber in concrete does not only provides an alternative aggregate source, but reduces landfill and tackles the associated health problems induced by burning rubber [11]. Therefore, many researches have been carried out to study the effect of crumb rubber on concrete properties [12,13]. In general, it was found that the major obstacle in using rubber in concrete is the weak bonding at the interfacial transition zone (ITZ) between the rubber particles and cementitious matrix, which, in turn, causes a significant reduction in compressive strength [14]. This strength reduction is related to the presence of cracks and voids surrounding rubber particles which weaken their performance. Based on Turki et al. [15], the thickness of the interface between the rubber and cement matrix increased with the increment of rubber content. Therefore, some researchers have tried to incorporate silica-based materials in rubberised cementitious material to overcome the loss of strength. Jokar et al. [16] used natural zeolite as the partial replacement of cement (5%, 10% and 15%) in order to enhance the mechanical properties of concrete containing rubber particles (1–6 mm) as the partial replacement of coarse aggregate. Based on their finding, the addition of zeolite has contributed to minimise the strength loss for all mixes. The compressive strength of concrete containing 10% rubber increased from 21 MPa to 33.5 MPa at 28 days with the addition of 15% zeolite, while the control mix (without rubber and zeolite) was 35 MPa. Ramdani et al. [17] also recorded a slight improvement of compressive strength in concrete incorporating both 10% crumb rubber (0.2–4 mm) and 15% glass powder compared to that of the control mix (without glass powder). Mhaya, Baharom [2], however, found a reasonable strength loss in concrete incorporating 10% recycled tire (1 – 4 mm) when palm oil fuel ash (POFA) was used as the partial replacement of cement (20%). It was concluded that void and gap increased with the increment of the rubber diameter. Henec, in this present study, the maximum size of used rubber was 900 μm and the maximum replacement percentage of sand by rubber was 8%.

In the same context, several researchers have also shifted their attention to utilise graphene and its derivative to substitute the loss of strength and minimise the ITZ in rubberised concrete. However, the majority of the previously published papers had only used graphene oxide (GO) to enhance the performance of rubberised concrete. Abdulkadir et al. [18] assessed the fresh properties of mortar containing fly ash, graphene oxide and crumb rubber at which GO was added as the replacement of cement (0.02%, 0.04%, 0.06%, and 0.08% by wt.), while crumb rubber was added as the replacement of fine aggregate (5%, 10% and 15% by volume). The results indicated that the flowability of the graphene-based mixes decreased compared to that of the control mixture. The decrement of flowability was linked to the GO particle as it is considered as hydrophobic. This fact is in line with Qureshi and Panesar [19], who demonstrated that the hydrophilic nature of GO and the oxygen functional groups in GO are responsible for the reduction in workability compared to that of the control mix (without GO). Hong et al. [20] also used GO to enhance the properties of engineered cementitious composite containing crumb rubber. It was found that the mechanical and deformable properties significantly increased. Furthermore, Abdulkadir et al. [21] evaluated the mechanical properties of engineered cementitious composite containing crumb rubber and GO. Based on the finding, the compressive, flexural and tensile strength were improved owing to the better bonding between crumb rubber and cement matrix. Despite various studies reporting increased mechanical properties of cementitious material with the addition of graphene oxide, one drawback was also recorded when using GO in which the excessive amount of oxygen functional groups in GO can create weakness zone inside the cement-based matrix due to agglomerates formation. This is because the positive charge of Ca^{2+}, Na^{+} and K^{+} exists inside the cement matrix and, hence, the negative charge of GO is able to agglomerate due to van der Waals forces [22].

Therefore, in this present study, graphene nanoplatelets was used to enhance the microstructure of rubberised mortar and substitute the strength loss. Silica fume was also added to produce further gel inside the cement-based matrix. The novelty of this present study, therefore, is to use both silica fume and graphene nanoplatelet in cement-based material (mortar) containing rubber powder with particle sizes ranging from 150 μm to 900 μm as fine aggregate replacement (2–8%). In addition, a mathematical model was developed using response surface methodology to obtain the optimum value of GnPs and rubber powder based on the best performance of the CS, FS, TS, porosity as well as UPV and WA of the proposed mortar. Microstructure tests involving scanning electron microscopy (SEM) were also conducted to examine the properties performance at micro and nano scale levels. Finally, this study will further increase and promote the use of rubber in cement-based materials in the construction industry.

2. Experimental and theoretical programs

2.1. Materials

Graphene nanoplatelets, cement, silica fume, natural sand, water, and chemical admixture are among the materials used in the proposed mortar. Graphene nanoplatelets and silica fume were purchased from GrapheneCA Inc. (US, NY) and Elkem Company, respectively. Cement I 52.5 R was collected from a local supplier that complies with Malaysian Standard MS 522 (2007) and ASTM C150 (2004). Table 1 presents the chemical composition of both cement and silica fume, which was determined using X-Ray fluorescence (XRF) spectroscopy. Tap water was used for mortar mixing, while a natural local sand was used as fine aggregate (FA), having a specific gravity of 2.64 and a maximum size of 2.36 mm that meet the grading requirements of fine aggregates according to (ASTM C

33–2003). In addition, a polycarboxylates superplasticizer was not only used to increase the workability of the mortar but also to enhance the dispersion of graphene nanoplatelets in water before mortar mixing. This fact was also confirmed by Papanikolaou et al. [23].

In addition, crumb rubber was collected from recycled waste tires after end-of-life service. Both shredders and shearing instruments were used to cut the discarded tyres into small fragments, followed by granular production using the micro-mill process. The maximum size of the crumb rubber particle was found to be 1.0 mm. Table 2 depicts the physical and chemical properties of the rubber used to replace the sand in the mortar.

2.2. Proportions of mortar mixture

The mortar's mixture proportion was designed in accordance with ASTM C 109 in which the cement-to-sand ratio (by mass) was 1:2.75, and the water-binder ratio was 0.4. The rubber was then added as partial replacement of natural sand (0%, 2%, 5%, and 8%) to the mixture, which was labeled as the control rubberised mortar (Mix 1, Mix 2, Mix 3, and Mix 4), respectively. Subsequently, the control rubberised mortar was incorporated with a 20% silica fume as additive (by volume), which was namely SF-based rubberised mortar. In particular, four mixes of SF-based rubberised mortar (Mix 5, Mix 6, Mix 7, and Mix 8) were developed and evaluated in which the rubber content was also 0%, 2%, 5% and 8%, respectively. The third class of the proposed mortar was the GnPs-SF-based rubberised mortar, which included both graphene nanoplatelets as binder replacement (0.02–0.6%) and rubber powder as fine aggregate replacement (2–8%). Nine experimental mixtures of GnPs-SF-based rubberised mortar (i.e., Mix 9 to Mix 17) were required according to the suggested values obtained from the response surface methodology, explained in the next section. Furthermore, the dosage of superplasticizer varied from 0.5% to 1% (by binder wt.) to maintain a consistent water content across all mixes for effective evaluation and comparison. Table 3 present the mixture proportions for the proposed mortar. It is worth noticing that the workability of mortar was kept at 180 mm ± 50 using the flow table for all mixture as shown in Fig. 1. The flow test was conducted based on ASTM C230.

2.3. Design of experiment

As there are two independent variables with varying percentages involving GnPs (0.02%–0.6%) and rubber powder (2%–8%), response surface methodology (RSM) was used to obtain the number of required experiments of the GnPs-SF-based rubberised mortar. RSM was also used to optimize the independent variables including, GnPs and rubber content (X_i) according to the target level of the output (Y_i) involving CS, FS, TS, P, UPV, and WA at the age 28 days. Indeed, RSM is regarded as one of the most commonly used optimization models in the present literature [24]. In recent years, optimization modelling of cement-based material using RSM gains a great attention in the civil engineering community. This is because that, with the aid of RSM optimization modelling, the number of experiments, the optimum value and the interaction between the involved parameters can be easily determined and evaluated [25,26]. RSM can also predict and optimize the properties of cement-based material with minimum errors [27]. Herein, Design Expert software was used to develop RSM optimization model. It is worth mentioning that the face-centered central composite design (FC-CCD) was adopted to generate the model.

In the same context, the relationship between the output and independent parameters was established using the quadratic formula. Eq. 1 represents the quadratic formula, where three coefficients (b_{ii}, bi and b_0) were used. These coefficients the represent quadratic, linear and the intercept of the model [28]. Various mathematical and statistical methods were used to assess the reliability and accuracy of the proposed formula. One of the most effective tools to assess the performance of the optimization model is the analysis of variance (ANOVA) such as p-value, F-value and the coefficient of determination (R^2). The mean absolute error (MAE), scatter index (SI), root mean square error (RMSE), mean absolute percentage error (MAPE) and root relative standard error (RRSE) were also employed to evaluate the effectiveness of the proposed models as shown in Eqs. (2–6) [29]. Where $\bar{Y}_a$ represents the average of the actual result, while the actual and predicted result was denoted by Y_a and Y_p, respectively, and N denotes the number of experiments.

$$Y = \beta_o + \sum_{i=1}^{k} \beta_i X_i + \sum_{i=1}^{k} \beta_{ii} X_i^2 + \sum_{i=1}^{k} \beta_{ij} X_{ij} \quad (1)$$

Table 1
XRF analysis of silica fume and cement.

Item	Mass percentage %	
	cement	SF
Al_2O_3	3.43	0.73
SiO_2	15.89	95.88
SO_3	4.41	0.21
CaO	68.88	0.31
K_2O	0.91	0.81
Fe_2O_3	3.89	0.19
MgO	0.97	0.43
Na_2O	0.081	0.25

Table 2
The chemical and physical properties of WTRCs.

Physical Properties	
Density	1.10 ± 0.1 kg/cm3
Bulk Density	0.41– 0.51 g/cm3
Hardness	50 – 70 Shore A
Tensile Strength	> 5 Mpa
Elongation at Break	> 500%
Passing (ASTM D5644)	> 80%
Heat Loss (ASTM D1509)	< 1 kgf/cm2
Metal Content (ASTM D5603)	< 0.5%
Fiber Content (ASTM D5603)	< 1 ML (Vr)
Chemical Properties	
Rubber hydrocarbon by difference	52%
Ash content	24%
Acetone extract	10%
Carbon black	14%

Table 3
Experimental test of the proposed mortar.

Type of mortar	No. mixture	Cement (kg/m^3)	SF (kg/m^3)	GnPs		Water (L/m^3)	FA (kg/m^3)	Rubber		admixture
				(%)	(kg)			(%)	(g)	(L)
Control rubberized mortar	Mix 1	530	-	-	-	212	1456	0	-	2.65
	Mix 2	530	-	-	-	212	1426.9	2	8	2.65
	Mix 3	530	-	-	-	212	1383.2	5	19	2.65
	Mix 4	530	-	-	-	212	1339.5	8	34	2.65
SF-based rubberized mortar	Mixt 5	506	101	-	-	243	1391	0	-	3.03
	Mix 6	506	101	-	-	243	1363	2	8	3.03
	Mix 7	506	101	-	-	243	1321	5	19	3.03
	Mix 8	506	101	-	-	243	1279	8	34	3.03
GnPs-SF-based rubberized mortar	Mix 9	506	101	0.31	1.88	243	1321	5	19	6.07
	Mix 10	506	101	0.02	0.121	243	1321	5	19	6.07
	Mix 11	506	101	0.31	1.88	243	1279	8	34	6.07
	Mixt 12	506	101	0.02	0.121	243	1279	8	34	6.07
	Mix 13	506	101	0.6	3.64	243	1363	2	8	6.07
	Mix 14	506	101	0.6	3.64	243	1279	8	34	6.07
	Mix 15	506	101	0.31	1.88	243	1363	2	8	6.07
	Mix 16	506	101	0.02	0.121	243	1363	2	8	6.07
	Mix 17	506	101	0.6	3.64	243	1321	5	19	6.07

Fig. 1. Slump test of the proposed mortar.

$$MAE = \frac{\sum |Y_p - Y_a|}{N} \tag{2}$$

$$SI = \frac{\sqrt{\frac{1}{n}\sum_{i=1}^{n}\left(Y_a - Y_p\right)^2}}{\bar{Y}_a} \tag{3}$$

$$RMSE = \sqrt{\frac{1}{N}\sum \left(Y_p - Y_a\right)^2} \tag{4}$$

$$MAPE = \frac{1}{n}\sum_{i=1}^{n}\left|\frac{Y_a - Y_p}{Y_a}\right| \tag{5}$$

$$RRSE = \sqrt{\frac{\sum \left(Y_p - Y_a\right)^2}{\sum \left(Y_p - \frac{1}{N}\sum Y_a\right)^2}} \tag{6}$$

2.4. Compressive strength test

The proposed mortars were evaluated using a compressive strength test at the age of 28 days. The test was conducted following the ASTM C109–109 M standards. Cubic samples (50 ×50 ×50 mm) were prepared and positioned on a compression machine following standard procedures. A constant load of 1200 N/s was also applied to the samples until they reached failure state. The recorded failure load was inserted in Eq. 7 to obtain the *CS* in MPa. Where *A* is the area of the cubic samples in mm^2 and *P* is the total applied load in N.

$$CS = \frac{P}{A} \tag{7}$$

2.5. Flexural strength test

ASTM C 348 was followed to determine the flexural strength of the proposed mortar. At the age of 28 days, a prism beam with a dimension of 40 × 40 × 160 mm was subjected to centre point loading. The clear span of the two support rollers was 120 mm, and the beam was loaded at a rate of 2.5 kN/min. Then, the flexural strength (*FS*) in MPa was calculated using Eq. 8.

$$FS = 0.0028P \tag{8}$$

2.6. Tensile strength test

ASTM C496/C496M was taken into account to obtain the splitting tensile strength of the proposed mortar. A cylinder sample with a dimension of 50 × 100 mm was employed to obtain the 28th-day split tensile strength. The sample was subjected to a constant loading rate of 1.0 MPa/min using a universal testing machine. The splitting strength (*TS*) in MPa was then determined using Eq. 9. where *L* is the cylinder length and *D* is the cylinder diameter.

$$TS = \frac{2P}{\pi DL} \tag{9}$$

2.7. Water absorption test

The percentage of water absorption of the proposed mortars at the age of 28 days was determined following the guidelines outlined in ASTM C642. Cubic samples with a dimension of (50 × 50 × 50) mm were used to carry out the test. First, the cubic cured samples were dried in the oven (110 °C) for 24 h and the oven dry mass (M_1) was weighed. The drying treatment was repeated at intervals of 24 h until the differences in successive values became lower than 0.5%. The samples were later submerged in a tap water container and weighed at saturation surface dry (M_2) every 24 h. This process was also repeated until a low difference (less than 0.5%) was achieved between two consecutive values. Finally, the water absorption (WA) was calculated using Eq. 10.

$$WA = \frac{M_2 - M_1}{M_1} \times 100 \tag{10}$$

2.8. Ultrasonic pulse velocity test

The ultrasonic pulse velocity test (UPV) is linked to the non-destructive technique family that assesses the target material without damage. UPV test is widely used in the civil engineering community due to its ability to evaluate the homogeneity of a cement-based material. With the aid of UPV, the quality of cementitious material and the crack propagation as well as the presence of pores can be assessed by measuring the velocity of the ultrasonic wave that passes through the material [30]. Herein, PUNDIT plus equipment, which features a receiver transducer and an emitter transducer with frequency of 54 kHz, was used to evaluate the proposed mortar. Cured cubic samples of (50 × 50 × 50 mm) at the age of 28 days were considered to conduct the test according to ASTM C 597–02. The pulse velocity was calculated according to Eq. 11, where *L* is the length of the sample that the wave passes through (m), while, *T* is the transmission time (s).

$$UPV = \frac{L_{(m)}}{T_{(s)}} \tag{11}$$

2.9. Porosity tests

The water-permeable porosity of GnPs-SF-based rubberised mortar was conducted at the age of 28 days and the porosity of this mortar was calculated according to vacuum saturation technique. Vacuum saturation technique is widely used to assess the amount of pores and voids inside the cement-based matrix [31]. This technique is similar to ASTM C 1202–05. It was performed using cubic samples having dimension of (50 × 50 × 50) mm. The target cubic samples were first oven-dried at 100 °C until a consistent weight was achieved (W_d). Then, three-hours vacuum pressure treatment was performed on the samples. Following that, the water was gradually introduced until the samples were completely submerged and kept for 24 h. After weighing the saturated samples (W_s), the total porosity was calculated using Eq. 12. Where W_d is the weight of dry samples. Furthermore, the weight of saturated samples in water was also measured and labelled as W_w.

$$porosity\left(\%\right) = \frac{W_s - W_d}{W_s - W_w} \tag{12}$$

2.10. Microstructure tests

Field emission scanning electron microscopy (FESEM) was considered to examine the performance of the proposed mortar at a micro and nano level. During the compressive strength test, a small specimen with a dimension not exceeding 1 cm was extracted from the cubic sample after they were crushed. The specimen was then dried in an oven having a temperature of 60 °C to eliminate the moisture content prior to FESEM test. Next, the specimens were coated with gold to enhance resolution. This microstructure test was

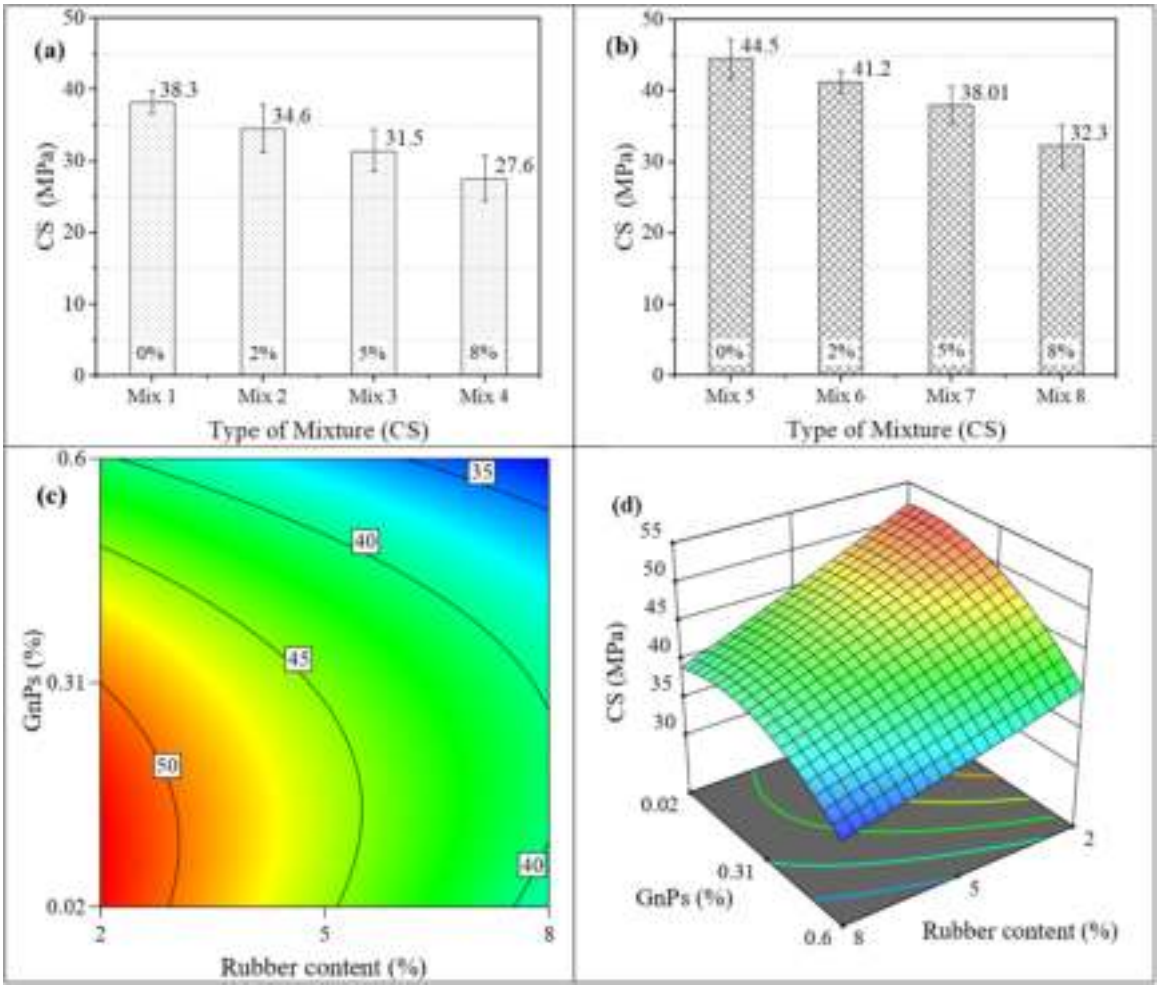

Fig. 2. Compressive strength evolution of (a) control rubberised mortar (b) SF-based rubberised mortar (c)(d) GnPs-SF-based rubberised mortar.

carried out using ZEISS MERLIN Field Emission Scanning Electron Microscopes, equipped with an energy dispersive X-ray analyser.

3. Results and discussion

3.1. Compressive strength

This section presents and elaborates on the compressive strength evolution of the proposed mortar at the age of 28 days. It is of note that the strength evolution was presented via three scenarios to effectively illustrate and emphasize the effect of rubber, SF, and SF+GnPs on the mortar's performance individually. In the first scenario, the compressive strength of the mortar incorporating rubber at different replacement percentages (0%, 2%, 5% and 8%) was conducted as shown in Fig. 2a, whereas, the inclusion of SF, and its impact on the control rubberised mortar's strength was presented in the second scenario as displayed in Fig. 2b. The combined influence of SF and GnPs on the strength performance of the rubberised mortar was visualised in the third scenario through a 2D counter plot and a 3D plot, depicted in Fig. 2c and d.

In scenario one (Fig. 2a), the compressive strength was gradually decreased with the increase of rubber content. The strength of control rubberised mortar containing 2% and 5% dropped by 9.7% (34.6 MPa) and 17.8% (31.5 MPa) respectively in comparison with the control one (38.3 MPa). In addition, the control rubberised mortar containing 8% rubber had the lowest compressive strength, measuring only 27.6 MPa. Overall, the obtained compressive strength of control rubberised mortar (without SF and GnPs) was lower than the strength of the control one. This noticeable and progressive decline in strength was attributed to several reasons. The gap and voids surrounding the rubber particles are regarded as the main reason to negatively affect the strength evolution. This is because they provide a vulnerable environment around the rubber particles, resulting in crack formation and ultimately damage to the concrete matrix when the load is applied. This fact is supported and discussed later in Section 3.7.2. The second potential reason is the softness of the rubber particles in comparison to the natural aggregate, which allows concrete cracks to spread during loading by providing an easy path for concrete fracture within the matrix. This fact is in a strong agreement with Shao et al. [32]. Abdelmonem et al. [12] also linked the strength reduction in rubberised concrete to the relatively soft nature of rubber particles compared to the cement paste and aggregate.

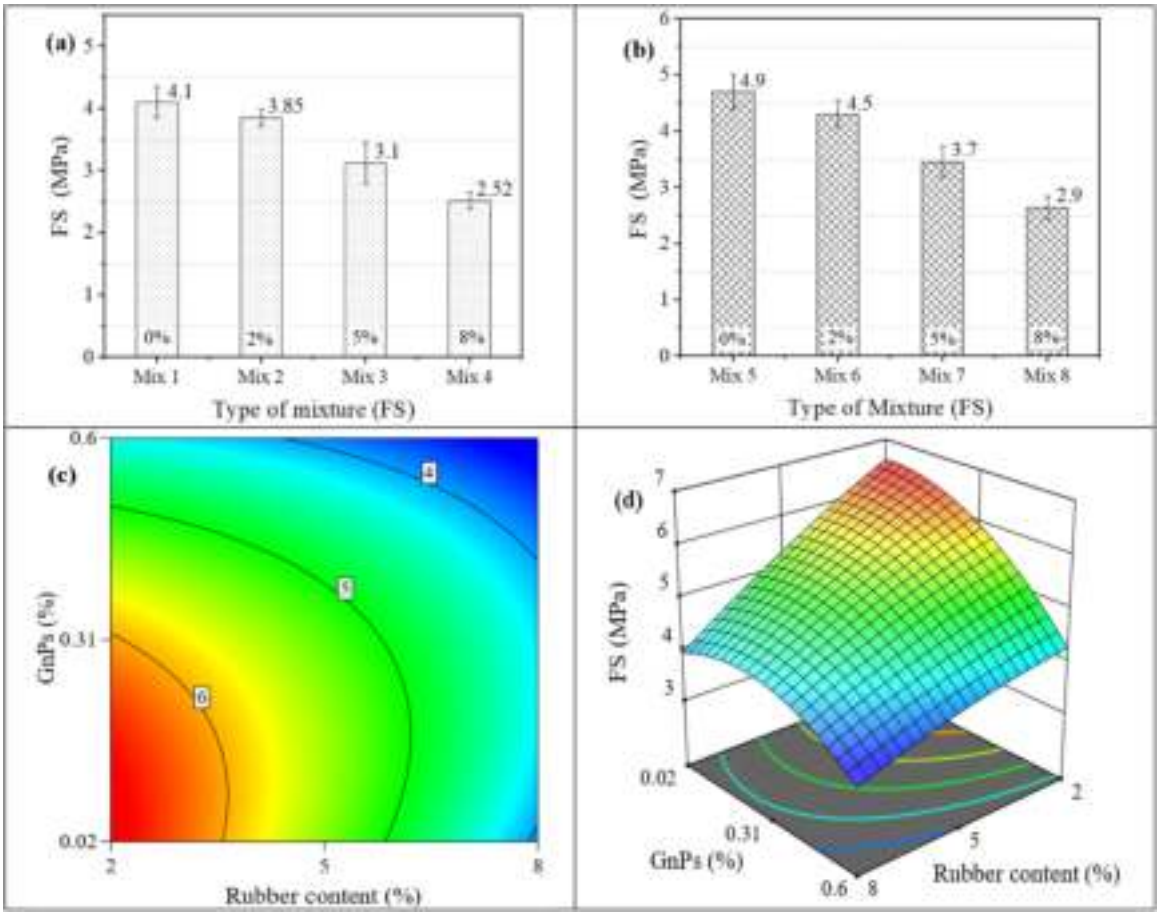

Fig. 3. Flexural strength evolution of (a) control rubberised mortar (b) SF-based rubberised mortar (c)(d) GnPs-SF-based rubberised mortar.

In the same context, the inclusion of SF in the rubberised mortar has a significant improvement, specifically, when the rubber content is small. With the addition of SF by 20%, the compressive strength of control mortar (without rubber) jumped from 38.3 MPa to 44.5 MPa. Moreover, the strength of the rubberised mortar increased from 34.6 MPa to 41.2 MPa at a rubber content of 2%. However, the effect of SF in rubberised mortar incorporating 8% is insignificant in which its compressive strength (32.3 MPa), which remained lower than that of the control one (38.3 MPa). This fact provides evidence to note that the efficiency of SF and its pozzolanic activity may not be sufficient to substitute the strength loss alone if the rubber content is high. Therefore, to minimise the pores and interfacial transition zone (ITZ) of rubberised mortar containing high rubber content (8% or more), another additive such as GnPs should be considered. Regardless, the strength improvement of the rubberised mortar mixture due to the addition of SF was attributed to the pozzolanic activity. SF is distinguished by its smaller particles and high surface area [33]. This advantage enables SF to quickly and fully react with calcium hydroxide $Ca(OH)_2$ even at an early age to ultimately induce Calcium silicate hydrates gel. This is also consistent with the previous work of Shi et al. [34].

On the other hand, based on Fig. 2c and 2 d, the value of compressive strength of GnPs-SF-based rubberized mortar is higher than the control mixture (38.3 MPa) for all replacement rubber percentage. For instance, the addition of 0.03% of GnPs increased the compressive strength of the proposed mortar incorporating 2% and 5% of rubber to 52.22 MPa and 45.51 MPa respectively. The proposed mortar containing 8% of rubber was also improved in which its strength jumped to 40.23 MPa in comparison with control rubberised mortar of only 27.6 MPa. That is, at a high rubber replacement percentage (8%), the contribution of GnPs to increasing compressive strength exceeds 32%, while the inclusion of SF alone has a small contribution (14.5%). Indeed, GnPs greatly enhanced and substituted the strength loss even under a high amount of rubber replacement percentage. This is justified by the fact that GnPs exhibited the ability to fill the pores and ITZ that was developed around the rubber particles. This is discussed in detail in Section 3.7.3. GnPs served as a filler material and could have a tensile strength reaching up 130 GPa [35]. GnPs acted to minimise the gap between the rubber particles and concrete matrix and have the ability to bond them to be one unity. However, a high content of GnPs does not

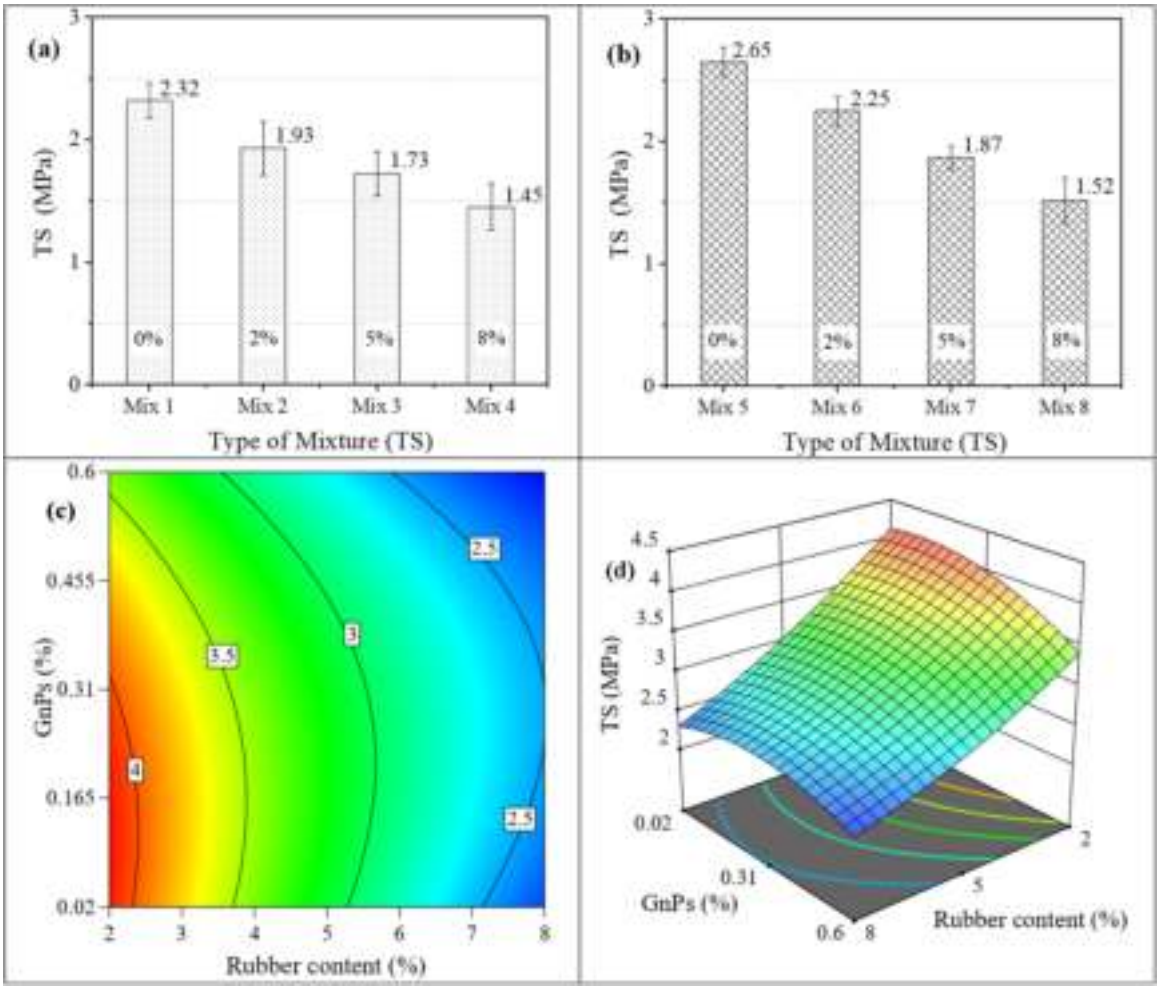

Fig. 4. Tensile strength evolution of rubberised concrete (a) control rubberised mortar (b) SF-based rubberised mortar (c)(d) GnPs-SF-based rubberised mortar.

contribute to any further strength improvement. This is in consistency with Shanmuga Priya et al. [36] who demonstrated that the better performance of concrete strength was achieved at 0.08% of graphene oxide. Ismail et al. [37] also found that optimum content of GnPs was 0.02% which increased tensile and compressive strength of concrete by 30.05% and 20.82% respectively.

3.2. Flexural strength

As shown in Fig. 3a, a similar trend was also observed in which the flexural strength was dropped with the increase of rubber content. The flexural strength was reduced by 6%, 24%, and 39% when the rubber content was 2%, 5%, and 8% respectively. This result was attributed to the generation of numerous microcracks around the rubber particles. These microcracks create a weaker area within the material that can potentially accommodate any further expected cracks during the loading. With the addition of SF, an improvement was recorded as illustrated in Fig. 3b. The value of flexural strength improvement varied according to the amount of rubber particles inside the mortar mixture. When the rubber content was 2% and 5%, the strength improvement was high at which the flexural strength jumped from 3.85 MPa to 4.5 MPa and from 3.12 MPa to 3.7 MPa respectively. A small enhancement in flexural strength was also observed when the rubber content is 8%.

Furthermore, as shown in Fig. 3c,d, it can be seen that the inclusion of GnPs significantly increased the flexural strength for all mixtures. For example, at 0.03% GnPs, the flexural strength of the mortar incorporating 2% and 5% jumped from 4.5 MPa to 6.5 MPa and from 3.7 MPa to 5.41 MPa respectively. This is a direct result as GnPs distributed and located around the rubber particles and acted as reinforcement providing additional strength and stability as discussed in details in Section 3.7.3. They also serve as a connector between the rubber particles and the cement-based matrix, as previously discussed. This bridging effect boosts the material's overall integrity and cohesion and resulting in the observed increase in compressive strength.

3.3. Tensile strength

Fig. 4 illustrates the tensile strength of the proposed mortar. It can be seen that a similar pattern was observed in Fig. 4a, where the tensile strength decreased as the rubber content increased. In the absence of SF and GnPs, the tensile strength of rubberised mortar dropped with the increase of rubber content. For instance, the tensile strength of control mortar (without rubber, SF, and GnPs) was 2.32 MPa, whereas, the inclusion of rubber content of 2%, 5%, and 8% resulted in decrement of tensile strength to 1.93 MPa, 1.73 MPa, and 1.45 MPa respectively. This anticipated outcome was related to the formation of cracks around the rubber particles (ITZ) when the load is applied, and finally caused the mortar to disintegrate as discussed earlier.

Fig. 4b, on the other hand, shows that the impact of SF on the tensile strength of rubberised mortar. Particularly, when the rubber component was 2%, 5%, and 8%, there was a corresponding loss in the tensile strength of 3%, 19%, and 34% respectively. Therefore, in the present study, the GnPs was used to fill the pores and minimize the ITZ. Based on Fig. 4d, the highest tensile strength was recorded at a lower percentage of GnPs. For instance, when 0.03% of GnPs were added to the mortar incorporating 8% of rubber content, the tensile strength increased significantly. The enhancement value was 22% in which it jumped from 1.52 MPa to 2.29 MPa. This enhancement was attributed to the presence of GnPs which acted as reinforcement within the cement matrix.

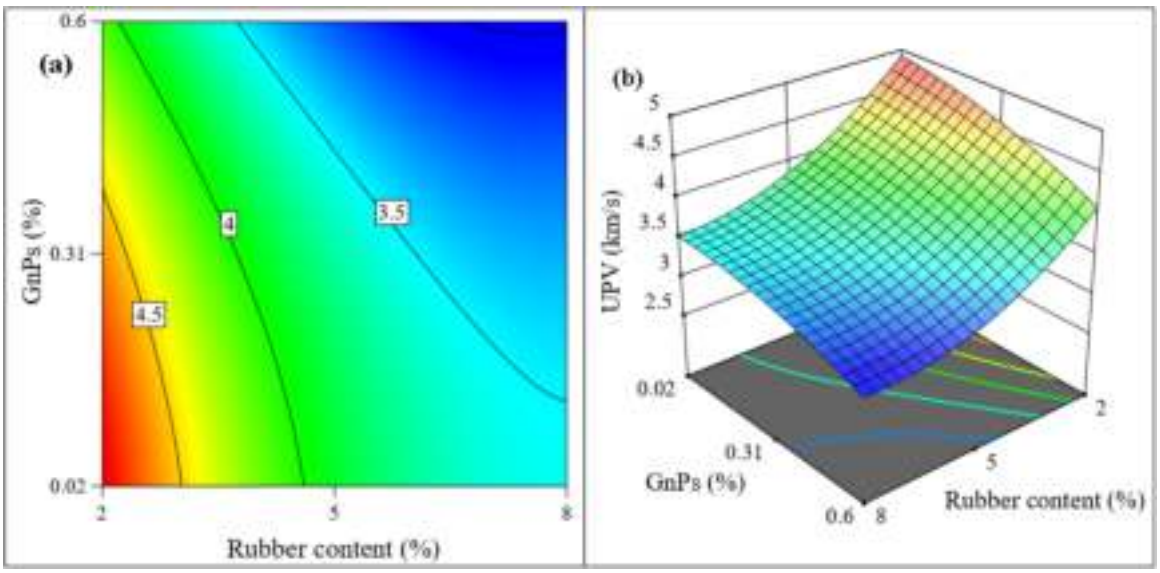

Fig. 5. UPV evolution of the GnPs-SF-based rubberised mortar.

3.4. UPV analysis

The values of the ultrasonic pulse velocity of the GnPs-SF-based rubberised mortar were calculated and presented in Fig. 5. The result of UPV has been widely used in the present literature. These values are regarded as significant indicators to assess the quality of concrete in terms of the presence of pores, defects, voids, and microcracks within the mortar matrix [38]. The higher value of UPV is associated with high-quality mortar, while the lowest values indicate a poor-quality mortar matrix. According to BS 1881, concrete quality can be considered as very good quality if the UPV value is greater than 4 km/s, while poor concrete could be achieved if the UPV value is lower than 3.0 km/s [39]. It can be seen that the GnPs-SF-based rubberised mortar can be classified as a good quality mortar for all levels of rubber replacement percentage. For instance, the UPV is almost higher than 3.89 km/s indicating a good quality mortar when the rubber content is 5%. This positive result was linked to the presence of GnPs that had ability to minimize the mortar pores as well as to stop the prorogation of microcracks within the mortar matrix. This fact was also supported by FESEM in Section 3.7.3.

3.5. Water absorption analysis

According to BS 1881–122:1983, water absorption of the cement-based matrix such as mortar or concrete can be defined as the additional weight of adsorbed water that was acquired compared to its dry state. Such increasement is attributed to the water capillary pressure inside the cement-based matrix when it is exposed to and immersed in water. Therefore, water absorption is another crucial parameter to evaluate concrete quality, specifically durability aspect. This is due to the fact that it is dependent on the movement of liquid within the cement-based matrix. A lower water absorption rate indicates denser and higher-quality concrete, whereas a higher absorption rate indicates a poor concrete. Based on ASTM C 642–06, the cement-based matrix can be considered to have an excellent

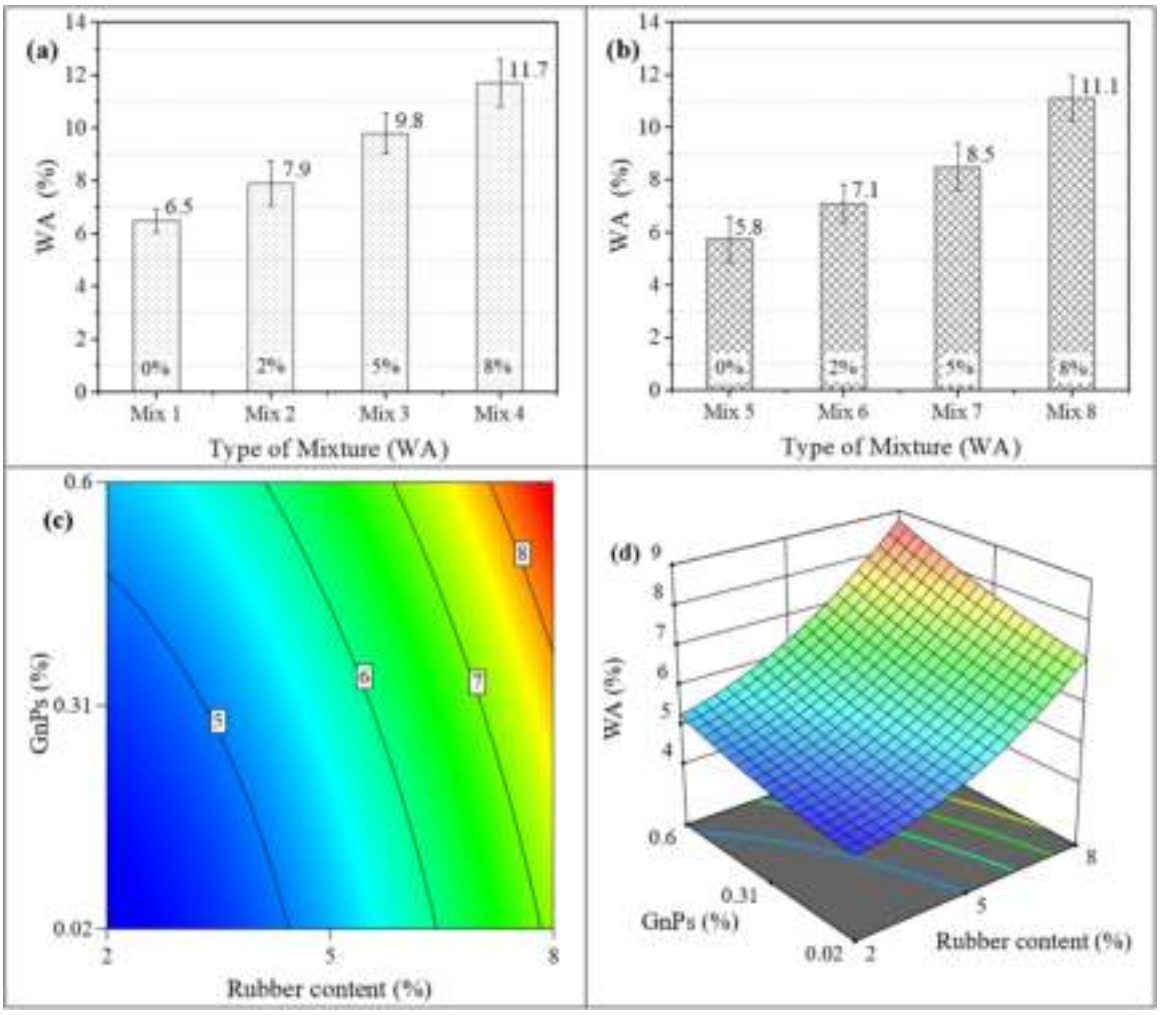

Fig. 6. Water absorption evolution of the proposed mortar (a) control rubberised mortar (b) SF-based rubberised mortar (c)(d) GnPs-SF-based rubberised mortar.

water absorption when its value is less than 5%. Moreover, a reasonable and good quality concrete can be obtained if the water absorption is less than 10% [40].

In the present study, it can be seen from Fig. 6a that the control rubberised mortar exhibited the highest water absorption level. For example, when the rubber content was 8% in a control rubberised mortar (without SF and GnPs), the *WA* was greater than 10%, indicating a poor-quality mortar. Water absorption decreased with the addition of silica fume, as shown in Fig. 6(b); however, the water absorption value did not meet the criteria for excellent concrete quality, as it remained in the range of 5–10%. The inclusion of both SF and graphene, on the other hand, resulted in significant water absorption reduction (less than 5%), indicating the achievement of excellent quality mortar, as shown in Fig. 6c, d.

3.6. Porosity test

The water-permeable porosity of the proposed mortar involving control rubberised mortar, SF-based rubberised mortar, and GnPs-SF-based rubberised mortar was respectively presented in Fig. 7a, b, c and d respectively. As can be seen in Fig. 7a, the control rubberised mortar had the highest porosity. This can be justified by that the cement matrix incorporates plenty of microcracks and pores in the area surrounding the rubber particles. The growing and interconnection of these microcracks and pores can create a convenient pathway for water to penetrate. In contrast, the porosity of the SF-based mortar containing 2% rubber was improved (8.65%) with the addition of silica fume compared to that of the control (10.57%), while the porosity of the SF-based mortar containing 8% rubber was 17.1% in comparison with control one (18.1%) as shown in Fig. 7a ,b.

On the other hand, the porosity decreased with the addition of GnPs for all mixtures as shown in Fig. 7c,d. For instance, the SF-based mortar containing 0.025% GnPs had the lowest porosity, with a value of 5.8%. This is consistent with the compressive strength result which was discussed in Section 3.1. The porosity of the GnPs-SF-based rubberised was the lowest overall. When the

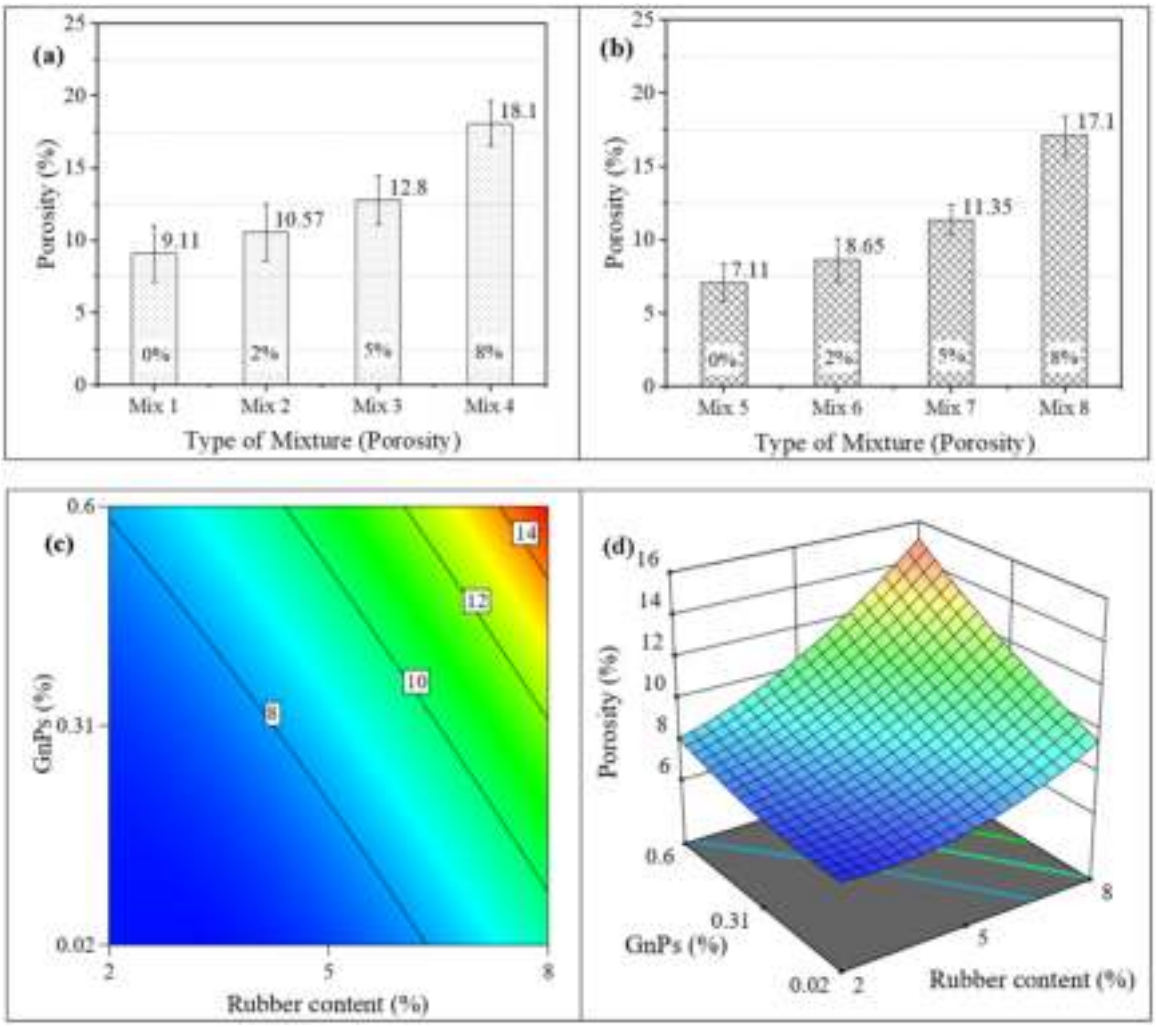

Fig. 7. Porosity evolution of the (a) control rubberised mortar (b) SF-based rubberised mortar (c)(d) GnPs-SF-based rubberised mortar.

rubber content was 2%, 5%, and 8%, the porosity was 5.8%, 7.78%, and 7.28%, respectively. The reduction in porosity was attributed to graphene's ability to prevent crack formation and propagation in the cement matrix. This point is addressed in Section 3.7.3.

3.7. Microstructure Analysis

3.7.1. Morphology of rubber and graphene

The morphology of rubber and GnPs was investigated and presented in Fig. 8. It can be observed that the GnPs consists of multiple layers of pristine graphene with a thickness ranging from 6 nm to 20 nm, while the average size of GnPs was found to be 11 μm as shown in Fig. 8a,b. This is almost in line with Jiang et al. [41] who stated that the average thickness and diameter of Graphene nanoplatelets are about 37 nm and 8 μm, respectively. Sánchez et al. [42] also defined the thickness of graphene nanoplatelets as being below 100 nm. Indeed, the thickness of GnPs plays a pivotal role in influencing the concrete properties. For instance, the thicker GnPs might be a good strategy to provide nucleation sites of the cement hydration products compared to that of the thinner pristine graphene. On the other hand, the shape of crumb rubber was to some extent irregular as shown in Fig. 8c. The average diameter of crumb rubber falls within the range of 150–900 μm. It is also remarkable to note that, according to SEM-EDX analysis, both GnPs and rubber contained high concentrations of carbon.

3.7.2. Interfacial transition zone between rubber and control mortar

It is worth mentioning that the interface between cement matrix and aggregate, which is well known as interfacial transition zone (ITZ), is a topic of significant interest. The presence of extensive porosity, microcracks, and calcium hydroxide within the ITZ makes it a weak zone within the cement-based matrix [43]. According to Wang and Dai [44], the ITZ is approximately distinguished by a thickness ranging from 20 to 100 μm. Fig. 9 shows the interface between the cement matrix and rubber. As depicted in Fig. 9a, a significant gap between the rubber and mortar was observed. Numerous microcracks surrounding the rubber particles were also observed. These microcracks have the potential to connect with existing pores and propagate as well as become larger cracks, posing a threat to the integrity of the cement matrix. It is also noted that the average interface thickness between rubber and cement gel was approximately 18 μm as illustrated in Fig. 9b. This is in a good agreement with Turki et al. [15] who found that the thickness of the interface between cement and rubber was 13.44 μm and the thickness value is dependent on the amount of rubber content in which it

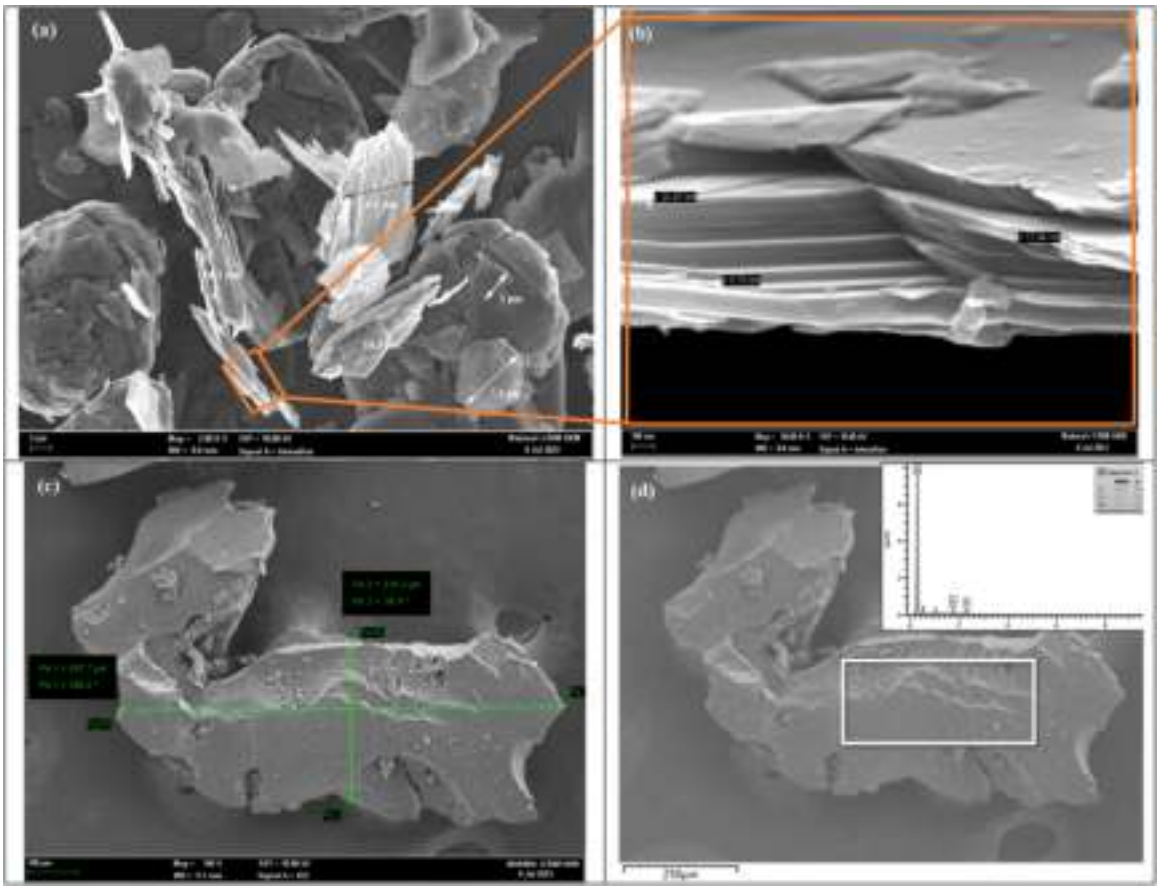

Fig. 8. Morphology of the rubber and GnPs using FESEM-EDX.

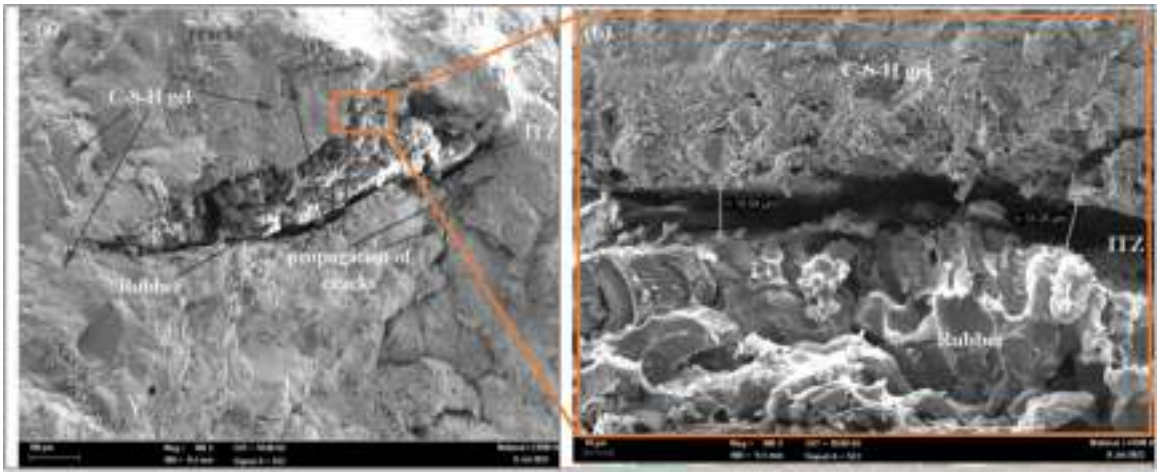

Fig. 9. The ITZ between rubber and cement matrix.

increased with the increase of rubber content.

3.7.3. ITZ and microstructure of the proposed mortar containing rubber and graphene

The ITZ between rubber and mortar matrix containing both silica fume and Graphene nanoplatelets (0.02%) was examined and evaluated using FE-SEM and EDX analysis as depicted in Fig. 10. According to Fig. 10 a, the darker color is associated with rubber particles, while the brighter colour is associated with calcium silicate hydrates gel (or C-S-H). This is also confirmed by the EDX

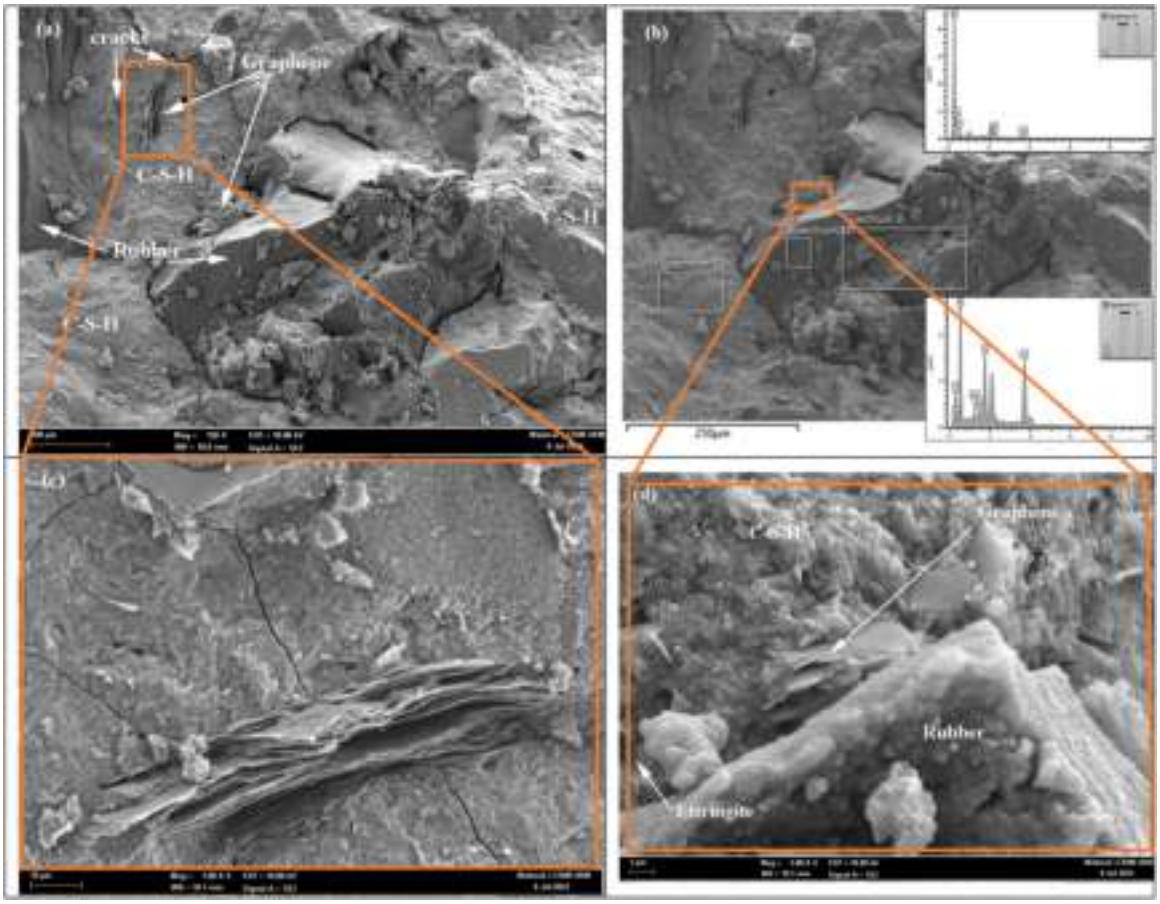

Fig. 10. ITZ and microstructure of the proposed GnPs-SF-based rubberised mortar.

analysis, which shows that the carbon concentration in the rubber particles was greater than 84.4%, as can be seen in Fig. 10 b. In contrast, the carbon content of cement gel is low (less than 9.0%). The C-S-H cement gel contains a high concentration of Ca, O, and Si. Furthermore, other chemical compounds found in cement gel included Al, Fe, K, and Mg. It is worth noting that the interface between the rubber and the cement gel is much smaller than that of the control rubberised mortar (without GnPs and SF). This is due to two reasons: firstly, the presence of silica fume which serves as micro filler [45], and the second reason is the presence of GnPs within the ITZ. GnPs, shown in Fig. 10 d, act as a nucleation site for the formation and development of cement gel.

Moreover, the presence of GnPs in the cement matrix plays an important role in preventing the spread of the inevitable microcracks. To be specific, the graphene nanoplatelets not only serve as a nano filler material, but also as an impermeable barrier to the continued propagation and growth of cracks where the cracks could not pass through the graphene nanoplatelets due to of the high strength of graphene, Fig. 10 c. Two significant advantages are noticed from the presence of graphene. First, it strengthens the cement matrix, while the second is that it reduces the ITZ.

3.8. Theoretical analysis

Six quadratic equations, listed in Table 4, were developed from the RSM model to investigate the CS, FS, TS, UPV, WA and *P* of the proposed rubberised mortar containing SF and GnPs at 28 days. These quadratic formulas are useful for quick understanding of the behaviour of the developed rubberised mortar and may be applicable for future prediction. The relationship between the output and the independent variables are examined by these formulas. They are also thought to be useful equations for determining the significance of their impact on the properties of the developed mortar.

The reliability of these equations was also investigated using ANOVA analysis and *p*-value as well as F-value as shown in Table 5. It can be seen that the *p*-value of the proposed equations is less than 0.05 confirming that the equations are significant and are able to predict the target properties with small error. This is line with Algaifi et al. [46] who used *p*-value to validate the developed quadratic equation of alkali activated mortar containing fly ash, slag and nano silica. F-value is also used to assess the significance of the mean value variance, in which a high F-value indicates a significant model. In the present study, F-value was found to be higher than 15 indicating that the models are significant.

To verify the accuracy of the above quadratic formulas, both the coefficient of determination (R^2) and the absolute relative deviation (*ARD*) were also utilised. This is because the former alone is insufficient to validate the model's accuracy. The R^2 could provide insight into the degree of similarity between predicted and actual results, while *ARD* revealed the error distribution within the proposed model. Both R^2 and error percentage (%) can be determined using Eqs. (13–14), respectively [28,47]. According to Habibi, Ramezanianpour [48], the proposed formula can be accepted if the value of error is lower than 10% and value of R^2 is higher than 0.9 [46]. For this cuurent study, as shown in Fig. 11, the value of R^2 was higher than 0.97 which revealed an appropriate and strong correlation between the experimental and predicted results. This finding concurs with Mokhtar et al. [49] who demonstrated that a strong correlation between the actual data and the experimental is achieved if the R^2 is higher than 0.7. In addition, the error percentage was less than 10% confirming that the proposed formulas can predict the experimental dataset with very small error, Fig. 11.

$$R^2 = \frac{\sum_{i=1}^{n}\left(Y_p - \bar{Y}_a\right)^2}{\sum_{i=1}^{n}\left(\bar{Y}_a - Y_a\right)^2} \tag{13}$$

$$Error = \left(\frac{actual - predicted}{actual}\right) \times 100 \tag{14}$$

Other mathematical and statistical indicators were also employed to verify the proposed equations as shown in Table 6. For instance, the ratio of R^2 to adjusted R^2 was close to one, and the differences between the predicted and adjusted R^2 values for all models were less than 0.2, indicating the accuracy and reasonableness of the mode. This is in agreement with Mohammed et al. [50]. Algaifi et al. [46] also stated that an excellent correlation can be achieved if the ratio between actual and predicted output is close to one. In the same context, the value of MAPE ranged was approximately 0.04 for all models indicating that the predicted output is reliable and can be used for further prediction. This finding is consistent with Getahun et al. [51] who found that the error difference between the actual and predicted compressive strength of concrete was 2.088%. Yaseen et al. [52], in turn, assessed the accuracy of the predicted shear strength of steel fiber-reinforced concrete beam using the scatter index (SI). They found that the SI ranged between 0.11 and

Table 4
The quadratic formulas for CS, TS, FS, UPV, WA and *P* of the rubberised mortar.

Eq. NO.	Output	The developed quadratic formulas
1	CS (MPa)	$CS = 56.71 - 2.4R + 4.45GnPs + 1.57R \times GnPs + 0.021R^2 - 44.97GnPs^2$
2	TS (MPa)	$TS = 4.9 - 0.45R + 0.34GnPs + 0.17R \times GnPs + 0.014R^2 - 3.05GnPs^2$
3	FS (MPa)	$FS = 7.27 - 0.313R - 0.53GnPs + 0.48R \times GnPs - 0.014R^2 - 7.19GnPs^2$
4	UPV (km/s)	$UPV = 5.97 - 0.59R - 0.703GnPs + 0.08R \times GnPs + 0.035R^2 - 1.5GnPs^2$
5	WA (%)	$WA = 4.5 - 0.16R - 0.13GnPs + 0.23R \times GnPs + 0.06R^2 + 1.78GnPs^2$
6	*P* (%)	$P = 7.73 - 0.64R - 3.37GnPs + 1.27R \times GnPs + 0.105R^2 + 4.7GnPs^2$

Table 5
ANOVA analysis of the proposed equations terms.

Item		Model	X_1	X_2	X_1X_2	X_1^2	X_2^2
CS	*p*-value	0.0243	0.0086	0.0125	0.2741	0.9048	0.0796
	F-value	15.17	38.09	29.15	1.78	0.0169	6.82
	Significant	*Y.*					
TS	*p*-value	0.009	0.0014	0.0522	0.1661	0.3441	0.1108
	F-value	30.42	132.71	9.77	3.32	1.26	5.02
	Significant	*Y.*					
FS	*p*-value	0.0242	0.0084	0.0147	0.0988	0.6509	0.0967
	F-value	15.22	38.70	25.82	5.6	0.2508	5.72
	Significant	*Y.*					
WA	*p*-value	0.0057	0.0010	0.0138	0.2624	0.0753	0.5182
	F-value	41.46	170.7	27.02	1.89	7.16	0.5329
	Significant	*Y.*					
UPV	*p*-value	0.0043	0.0009	0.0052	0.2975	0.029	0.2276
	F-value	49.99	176.28	54.23	1.58	15.56	2.29
	Significant	*Y.*					
P	*p*-value	0.0059	0.0016	0.0045	0.0264	0.0910	0.3797
	F-value	40.7	119.43	60.2	16.76	6.05	1.06
	Significant	*Y.*					

0.27confirming that the module is accurate. In this present study, SI was found to be lesser than 0.04 for all models.

Furthermore, the desirability function (DR) was employed to explore the optimum mix design for the proposed rubberised mortar. The optimal content of rubber particles and graphene nanoplatelets, in particular, was determined using the desirability function. This is because the desirability function has been identified as a highly effective and successful approach for optimisation [48]. For the purpose of this study, three scenarios were adopted to find out the optimal content. The initial scenario was to obtain the content of GnPs and rubber content resulting in the highest CS, TS, FS, and UPV as well as the lowest values of WA and *P*. The second scenario was concerned with achieving the highest possible rubber content while still maintaining acceptable levels of CS, TS, and FS, UPV, WA and *P*. Lastly, the third scenario aimed to find the optimum content of rubber and GnPs that resulted in good and acceptable properties.

Table 7 presents the optimal values of GnPs and rubber according to these three scenarios. Excellent and highest mortar properties can be obtained by keeping the rubber content at a low percentage (2%) and adding GnPs at a concentration of 0.03%. The compressive strength in this scenario is 52.22 MPa, which is significantly higher than the control mortar's compressive strength of 38.3 MPa. In scenario two, the compressive strength of the mortar containing 8% rubber and 0.03% GnPs measured 40.21 MPa, which is still higher the compressive strength of the control mortar. In scenario 3, it can be seen that the optimal value of rubber and GnPs was 5% and 0.03% in which good properties were achieved.

4. Conclusion

This study aimed to assess the performance of rubberised mortar incorporating GnPs and SF based on its CS, TS, CS, *P* as well as WA and UPV. Based on the outcomes, the following conclusions could be drawn:

i. The rubberized mortar incorporating SF and GnPs consistently displayed superior properties in comparison to the control mixture, regardless of the percentage of rubber replacement.
ii. The optimum content of GnPs content was 0.03%, while a high-level content of GnPs did not contribute to an increase in strength.
iii. FESEM images revealed the ability of GnPs to enhance the mortar's microstructure and the ITZ between the rubber and cement matrix.
iv. The RSM model showed its ability to predict accurate result in which MAPE and SI were less than 0.11.

Conflict of interest

The authors whose names are listed immediately below certify that they have NO affiliations with or involvement in any organization or entity with any financial interest (such as honoraria; educational grants; participation in speakers' bureaus; membership, employment, consultancies, stock ownership, or other equity interest; and expert testimony or patent-licensing arrangements), or non-financial interest (such as personal or professional relationships, affiliations, knowledge or beliefs) in the subject matter or materials discussed in this manuscript.

Declaration of Competing Interest

The authors declare that they have no known competing financial interests or personal relationships that could have appeared to influence the work reported in this paper.

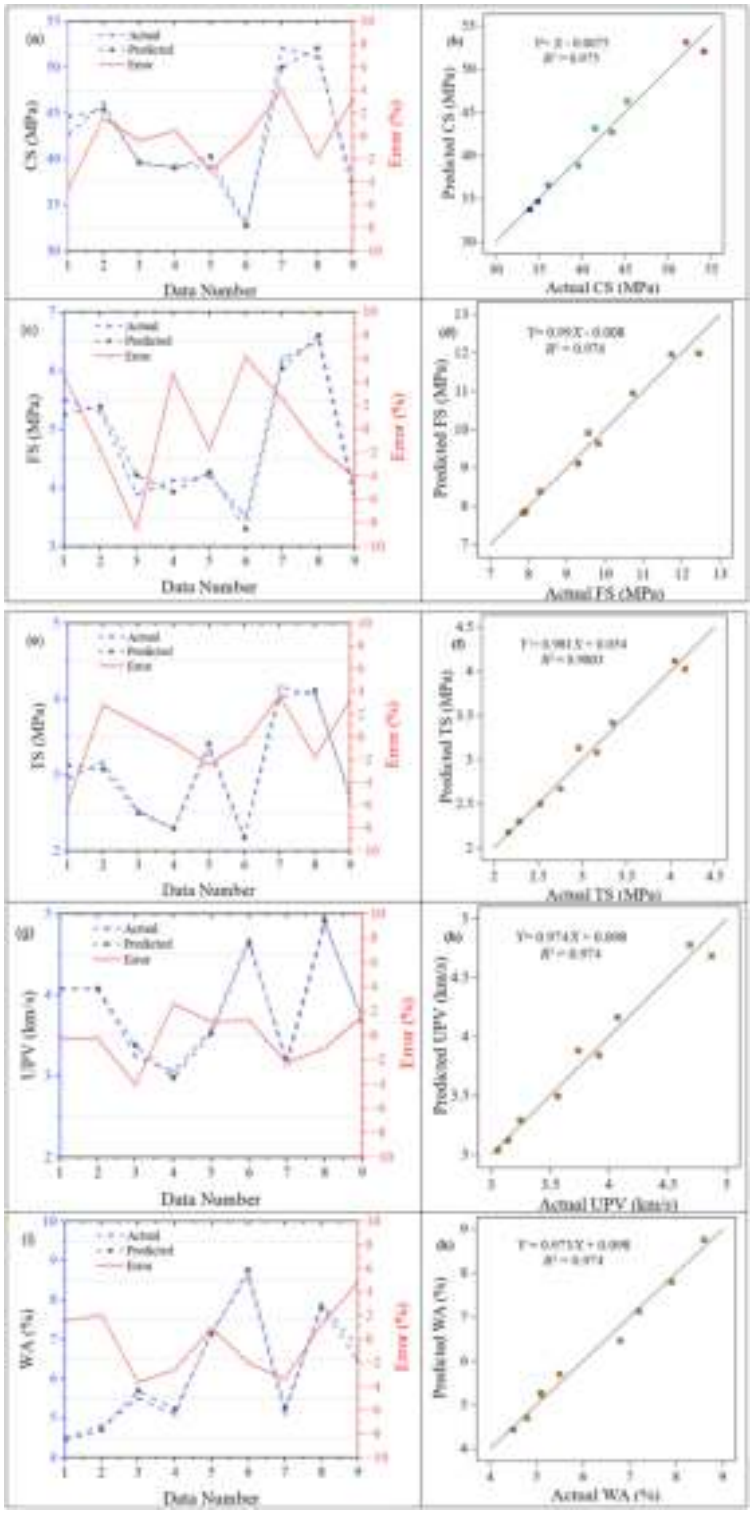

Fig. 11. Verification of the proposed formulas (a)(b) CS (c)(d) FS (e)(f) TS (g)(h) UPV (i)(k) WA.

Data Availability

Data will be made available on request.

Table 6
Statistical and mathematical indicators to validate the proposed formulas.

Item	Output					
	CS	FS	TS	UPV	WA	porosity
Adjusted R^2	0.8985	0.8989	0.9484	0.9684	0.962	0.9855
Predicted R^2	0.7588	0.775	0.8442	0.8673	0.8502	0.8573
Adeq. Precision	11.57	11.303	14.65	20.64	18.26	18.687
SI	0.028	0.0399	0.0309	0.0173	0.027	0.033
MAPE	0.021	0.0394	0.024	0.0159	0.025	0.029
MAE	0.947	0.1738	0.0778	0.056	0.149	0.254
RRSE	0.0295	0.0418	0.0321	0.0183	0.0278	0.032
RMSE	1.18	0.1908	0.0943	0.066	0.168	0.312

Table 7
Optimization using desirability function.

No.	Optimal content		Mortar properties					
	Graphene (%)	Rubber (%)	CS (MPa)	FS (MPa)	TS (MPa)	UPV (km/s)	WA (%)	*P* (%)
Scenario 1	0.030	2	52.22	6.57	4.14	4.87	4.45	6.78
Scenario 2	0.030	8	40.21	4.01	2.31	3.52	7.13	9.48
Scenario 3	0.03%	5	45.51	5.41	3.13	3.89	5.23	7.28

Acknowledgement

The authors would like to acknowledge the support of this research by the Deputy for Research and Innovation Ministry of Education, the Kingdom of Saudi Arabia, through grant number (NU/IFC/2/SERC/-/8) under the Institutional Funding Committee at Najran University, the Kingdom of Saudi Arabia. Also, the authors would like to express their gratitude to the Ministry of Higher Education of Malaysia and Universiti Kebangsaan Malaysia for providing funding to this project with the grant number: GUP-2022–029. Moreover, this work was also supported by Dato' Low Tuck Kwong International Grant under project code of 20238002DLTK.

References

[1] Z.S. Adnan, et al., Performance of rice husk ash as a material for partial cement replacement in concrete, Mater. Today.: Proc. 48 (2022) 842–848.
[2] A.M. Mhaya, et al., Systematic experimental assessment of POFA concrete incorporating waste tire rubber aggregate, Polymers 14 (11) (2022) 2294.
[3] H.A. Algaifi, et al., Mechanical properties of coconut shell-based concrete: experimental and optimisation modelling, Environ. Sci. Pollut. Res. 29 (14) (2022) 21140–21155.
[4] M. Amran, et al., Global carbon recoverability experiences from the cement industry, Case Stud. Constr. Mater. 17 (2022), e01439.
[5] D.G. Gokhale, A.A. Kaish, Recent trends in incorporating graphene coated sand in self-sensing cementitious composites, Mater. Proc. 14 (1) (2023) 48.
[6] H. Alhawat, et al., Assessing the quality of concrete tunnel lining exposed to tunnel fire through residual compressive strength, Adv. Civ. Eng. 2023 (2023).
[7] A. Syamsir, et al., Performance analysis of full assembly glass fiber-reinforced polymer composite cross-arm in transmission tower, Polymers 14 (8) (2022) 1563.
[8] A.M. Mhaya, et al., Systematic evaluation of permeability of concrete incorporating coconut shell as replacement of fine aggregate, Materials 15 (22) (2022) 7944.
[9] A.M. Mhaya, et al., Evaluating mechanical properties and impact resistance of modified concrete containing ground Blast Furnace slag and discarded rubber tire crumbs, Constr. Build. Mater. 295 (2021), 123603.
[10] R. Othman, et al., Evaluation on the rheological and mechanical properties of concrete incorporating eggshell with tire powder, J. Mater. Res. Technol. 14 (2021) 439–451.
[11] Y.-c Guo, et al., Compressive behaviour of concrete structures incorporating recycled concrete aggregates, rubber crumb and reinforced with steel fibre, subjected to elevated temperatures, J. Clean. Prod. 72 (2014) 193–203.
[12] A. Abdelmonem, et al., Performance of high strength concrete containing recycled rubber, Constr. Build. Mater. 227 (2019), 116660.
[13] K. Bisht, P. Ramana, Evaluation of mechanical and durability properties of crumb rubber concrete, Constr. Build. Mater. 155 (2017) 811–817.
[14] J. Wang, et al., Effects of ages on the ITZ microstructure of crumb rubber concrete, Constr. Build. Mater. 254 (2020), 119329.
[15] M. Turki, et al., Microstructure, physical and mechanical properties of mortar–rubber aggregates mixtures, Constr. Build. Mater. 23 (7) (2009) 2715–2722.
[16] F. Jokar, et al., Experimental investigation of mechanical properties of crumbed rubber concrete containing natural zeolite, Constr. Build. Mater. 208 (2019) 651–658.
[17] S. Ramdani, et al., Physical and mechanical performance of concrete made with waste rubber aggregate, glass powder and silica sand powder, J. Build. Eng. 21 (2019) 302–311.
[18] I. Abdulkadir, et al., Effects of graphene oxide and crumb rubber on the fresh properties of self-compacting engineered cementitious composite using response surface methodology, Materials 15 (7) (2022) 2519.
[19] T.S. Qureshi, D.K. Panesar, Impact of graphene oxide and highly reduced graphene oxide on cement based composites, Constr. Build. Mater. 206 (2019) 71–83.
[20] D.L. Hau Hong, et al., Deformation properties of rubberized ecc incorporating nano graphene using response surface methodology, Materials 13 (12) (2020) 2831.
[21] I. Abdulkadir, et al., Modelling and optimization of the mechanical properties of engineered cementitious composite containing crumb rubber pretreated with graphene oxide using response surface methodology, Constr. Build. Mater. 310 (2021), 125259.
[22] K. Amini, et al., Evaluation of the dispersion of metakaolin–graphene oxide hybrid in water and cement pore solution: can metakaolin really improve the dispersion of graphene oxide in the calcium-rich environment of hydrating cement matrix? RSC Adv. 11 (30) (2021) 18623–18636.

[23] I. Papanikolaou, et al., Investigation of the dispersion of multi-layer graphene nanoplatelets in cement composites using different superplasticiser treatments, Constr. Build. Mater. 293 (2021), 123543.
[24] A. Hammoudi, et al., Comparison of artificial neural network (ANN) and response surface methodology (RSM) prediction in compressive strength of recycled concrete aggregates, Constr. Build. Mater. 209 (2019) 425–436.
[25] H.A. Algaifi, et al., Strength and acid resistance of ceramic-based self-compacting alkali-activated concrete: optimizing and predicting assessment, Materials 14 (20) (2021) 6208.
[26] V. Anggraini, et al., Response surface methodology: the improvement of tropical residual soil mechanical properties utilizing calcined seashell powder and treated coir fibre, Sustainability 15 (4) (2023) 3588.
[27] M.Y.M. Al-Fasih, et al., Synthesis of rubberized alkali-activated concrete: experimental and numerical evaluation, Constr. Build. Mater. 303 (2021), 124526.
[28] H.A. Algaifi, et al., Machine learning and RSM models for prediction of compressive strength of smart bio-concrete, Smart Struct. Syst. 28 (2021) 535–551.
[29] H.A. Salah, et al., Assessment of the mechanical properties of high strength mortar incorporating silica fume and graphene nanoplatelets: experimental and mathematical modeling, Sustainability 15 (10) (2023) 8054.
[30] I. Hager, M. Sitarz, K. Mróz, Fly-ash based geopolymer mortar for high-temperature application–effect of slag addition, J. Clean. Prod. 316 (2021), 128168.
[31] A. Rahul, et al., Mechanical characterization of 3D printable concrete, Constr. Build. Mater. 227 (2019), 116710.
[32] J. Shao, et al., Combined effect of recycled tire rubber and carbon nanotubes on the mechanical properties and microstructure of concrete, Constr. Build. Mater. 322 (2022), 126493.
[33] H.A. Salah, et al., Development of ultra-high-performance silica fume-based mortar incorporating graphene nanoplatelets for 3-dimensional concrete printing application, Buildings 13 (8) (2023) 1949.
[34] C. Shi, et al., The hydration and microstructure of ultra high-strength concrete with cement–silica fume–slag binder, Cem. Concr. Compos. 61 (2015) 44–52.
[35] T. Dayyoub, et al., The structure and mechanical properties of the UHMWPE films modified by the mixture of graphene nanoplates with polyaniline, Polymers 11 (1) (2018) 23.
[36] T. Shanmuga Priya, et al., Effect of graphene oxide on high-strength concrete induced with rice husk ash: mechanical and durability performance, Innov. Infrastruct. Solut. 6 (2021) 1–16.
[37] F.I. Ismail, et al., Behavioral assessment of graphene nanoplatelets reinforced concrete beams by experimental, statistical, and analytical methods, Case Stud. Constr. Mater. 17 (2022), e01676.
[38] M.S. Nasr, et al., Properties of eco-friendly cement mortar contained recycled materials from different sources, J. Build. Eng. 31 (2020), 101444.
[39] I.T. Yusuf, Y.A. Jimoh, W.A. Salami, An appropriate relationship between flexural strength and compressive strength of palm kernel shell concrete, Alex. Eng. J. 55 (2) (2016) 1553–1562.
[40] K.H. Mo, et al., Viability of agricultural wastes as substitute of natural aggregate in concrete: a review on the durability-related properties, J. Clean. Prod. 275 (2020), 123062.
[41] Z. Jiang, O. Sevim, O.E. Ozbulut, Mechanical properties of graphene nanoplatelets-reinforced concrete prepared with different dispersion techniques, Constr. Build. Mater. 303 (2021), 124472.
[42] M. Sánchez, et al., Effect of graphene nanoplatelets thickness on strain sensitivity of nanocomposites: a deeper theoretical to experimental analysis, Compos. Sci. Technol. 181 (2019), 107697.
[43] J. He, D. Lei, W. Xu, In-situ measurement of nominal compressive elastic modulus of interfacial transition zone in concrete by SEM-DIC coupled method, Cem. Concr. Compos. 114 (2020), 103779.
[44] Y.-S. Wang, J.-G. Dai, X-ray computed tomography for pore-related characterization and simulation of cement mortar matrix, NDT E Int. 86 (2017) 28–35.
[45] P. Akarsh, S. Marathe, A.K. Bhat, Influence of graphene oxide on properties of concrete in the presence of silica fumes and M-sand, Constr. Build. Mater. 268 (2021), 121093.
[46] H.A. Algaifi, et al., Optimisation of GBFS, fly ash, and nano-silica contents in alkali-activated mortars, Polymers 13 (16) (2021) 2750.
[47] D. Fan, et al., Precise design and characteristics prediction of ultra-high performance concrete (UHPC) based on artificial intelligence techniques, Cem. Concr. Compos. 122 (2021), 104171.
[48] A. Habibi, et al., RSM-based evaluation of mechanical and durability properties of recycled aggregate concrete containing GGBFS and silica fume, Constr. Build. Mater. 270 (2021), 121431.
[49] N. Mokhtar, et al., A sustainable enhancement of bio-cement using immobilised Bacillus sphaericus: optimization, microstructural properties, and techno-economic analysis for a cleaner production of bio-cementitious mortars, J. Clean. Prod. 318 (2021), 128470.
[50] B.S. Mohammed, V.C. Khed, M.F. Nuruddin, Rubbercrete mixture optimization using response surface methodology, J. Clean. Prod. 171 (2018) 1605–1621.
[51] M.A. Getahun, S.M. Shitote, Z.C.A. Gariy, Artificial neural network based modelling approach for strength prediction of concrete incorporating agricultural and construction wastes, Constr. Build. Mater. 190 (2018) 517–525.
[52] Z.M. Yaseen, et al., Shear strength prediction of steel fiber reinforced concrete beam using hybrid intelligence models: a new approach, Eng. Struct. 177 (2018) 244–255.